HHS Public Access

Author manuscript

Stem Cells. Author manuscript; available in PMC 2018 December 01.

Published in final edited form as:

Stem Cells. 2017 December ; 35(12): 2366–2378. doi:10.1002/stem.2707.

Gene-edited human kidney organoids reveal mechanisms of disease in podocyte development

Yong Kyun Kim[1,2,3,4,*], **Ido Refaeli**[5,6,*], **Craig R. Brooks**[7,*], **Peifeng Jing**[8], **Ramila E. Gulieva**[1,2,3,4], **Michael R. Hughes**[5,6], **Nelly M. Cruz**[1,2,3,4], **Yannan Liu**[8], **Angela J. Churchill**[1,2,3,4], **Yuliang Wang**[3,9], **Hongxia Fu**[3,4,10,11], **Jeffrey W. Pippin**[1,4], **Lih Y. Lin**[8], **Stuart J. Shankland**[1,4], **A. Wayne Vogl**[12], **Kelly M. McNagny**[5,6,†], and **Benjamin S. Freedman**[1,2,3,4,†]

[1]Division of Nephrology, University of Washington School of Medicine, Seattle WA 98109, USA

[2]Kidney Research Institute, University of Washington School of Medicine, Seattle WA 98109, USA

[3]Institute for Stem Cell and Regenerative Medicine, University of Washington School of Medicine, Seattle WA 98109, USA

[4]Department of Medicine, University of Washington School of Medicine, Seattle WA 98109, USA

[5]The Biomedical Research Centre, University of British Columbia, Vancouver V6T 1Z3, British Columbia, Canada

[6]Department of Medical Genetics, University of British Columbia, Vancouver V6T 1Z3, British Columbia, Canada

[7]Division of Nephrology, Vanderbilt University School of Medicine, Nashville TN 37232

[8]Department of Electrical Engineering, University of Washington, Seattle WA 98109, USA

[9]Paul G. Allen School of Computer Science and Engineering, University of Washington, Seattle, Washington, 98195, USA

[10]Division of Hematology, Department of Medicine, University of Washington School of Medicine, Seattle WA 98109, USA

[11]Department of Bioengineering, University of Washington School of Medicine, Seattle WA 98109, USA

[12]Department of Cellular and Physiological Sciences, University of British Columbia, Vancouver V6T 1Z3, British Columbia, Canada

[†]Corresponding authors: CONTACT INFORMATION: Benjamin S. Freedman, Ph.D., Assistant Professor of Medicine, University of Washington School of Medicine, Division of Nephrology, 850 Republican St, Box 358056, Seattle, WA 98109, USA, Phone: +1 (206) 685-4653, benof@uw.edu. Kelly M. McNagny, Ph.D., Professor of Medical Genetics, Co-Director of the Biomedical Research Centre, Scientific Director for the Centre for Drug Research and Development (CDRD), University of British Columbia, Vancouver V6T 1Z3, Phone: +1 (604) 822-7824, kelly@brc.ubc.ca.

[*]These authors contributed equally to this work

AUTHOR CONTRIBUTIONS

YKK, CRB, REG, NM, AJC, JP, SJS, and BSF performed experiments in human cells and tissues. IR, AWV, MH, and KMM performed experiments in podocalyxin knockout mice. PJ, YL, REG, NM, BSF, and LYL performed optical tweezers experiments. HF and BSF performed electrostatic force analysis. YW and BSF performed RNA-Seq analysis. BSF wrote the manuscript with input from all of the authors.

Abstract

A critical event during kidney organogenesis is the differentiation of podocytes, specialized epithelial cells that filter blood plasma to form urine. Podocytes derived from human pluripotent stem cells (hPSC-podocytes) have recently been generated in nephron-like kidney organoids, but the developmental stage of these cells and their capacity to reveal disease mechanisms remains unclear. Here we show that hPSC-podocytes phenocopy mammalian podocytes at the capillary loop stage (CLS), recapitulating key features of ultrastructure, gene expression, and mutant phenotype. hPSC-podocytes *in vitro* progressively establish junction-rich basal membranes (nephrin^{+}podocin^{+}ZO-1^{+}) and microvillus-rich apical membranes (podocalyxin^{+}), similar to CLS podocytes *in vivo*. Ultrastructural, biophysical, and transcriptomic analysis of gene-edited hPSCs and derived podocytes, generated using CRISPR/Cas9, reveals that podocalyxin is essential for the assembly of microvilli and lateral spaces between developing podocytes. These defects are phenocopied in CLS glomeruli of podocalyxin-deficient mice, which cannot produce urine, thereby demonstrating that podocalyxin has a conserved and essential role in mammalian podocyte maturation. Defining the maturity of hPSC-podocytes and their capacity to reveal and recapitulate pathophysiological mechanisms establishes a powerful framework for studying human kidney disease and regeneration.

Graphical abstract

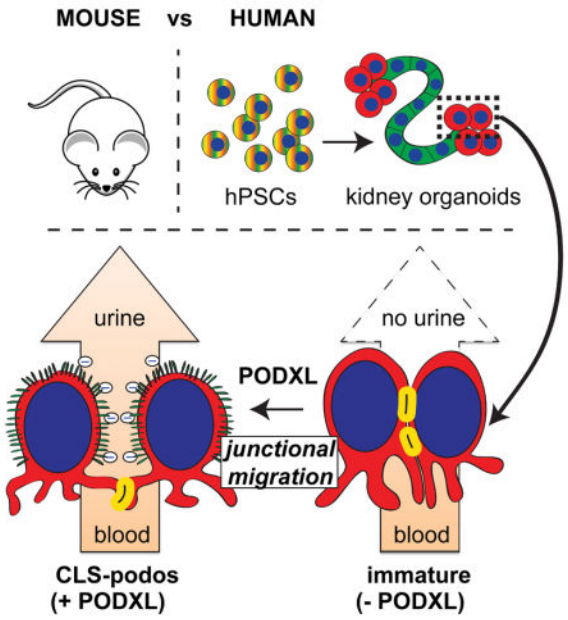

Comparison of stem cell-derived human kidney organoids *in vitro* with genetic mouse models *in vivo* reveals that podocytes (red), the filtering cells of the kidney, undergo apical-to-basal junctional migration at the capillary loop stage (CLS). A critical player in this process is podocalyxin (PODXL), which induces negatively-charged microvilli between neighboring podocytes, pushing them apart.

Keywords

Pluripotent stem cells; kidney; adhesion receptors; CRISPR; differentiation; gene targeting; developmental biology; iPS cells; focal segmental glomerulosclerosis; nephrogenesis; cell adhesion; foot processes; slit diaphragm; PODXL; NPHS1; NPHS2; PAX2; PAX8; WT1; SYNPO; ZO-1; genome editing; biophysics

INTRODUCTION

Humans are born with a fixed number of kidney subunits, called nephrons. Progressive and irreversible reduction in nephron number causes end-stage renal disease, affecting two million people worldwide, in which kidney function fails, and either dialysis or kidney transplant is required to sustain life. These treatments are of limited availability and efficacy, prompting interest in new therapeutic strategies based on the expansion of nephron progenitor cell populations that arise during kidney development [1–5], with the ultimate goal of generating new kidney tissues for transplantation [6–9].

Human pluripotent stem cells, or hPSCs, are both self-renewing and pluripotent, providing a renewable source of diverse cells and tissues for laboratory studies and regeneration [10, 11]. hPSCs include both embryonic stem cells (ESCs) derived from embryos and induced pluripotent stem cells (iPSCs) reprogrammed from adult cells. Recently, multiple groups have published protocols describing the generation of kidney tissues from hPSCs [3–5]. In these protocols, hPSCs differentiate stepwise, first into primitive streak mesendoderm, subsequently into nephron progenitor cells expressing *sine oculis-related 2* (*SIX2*), and finally into organoids containing segments of distal tubules, proximal tubules, and podocytes [3–5, 12–14]. This provides a new resource for modeling human kidney disease and regeneration.

The generation of hPSC-derived podocytes (hPSC-podocytes) in these cultures is particularly interesting because primary podocytes are highly specialized, terminally differentiated epithelial cells that have been challenging to study *in vitro* or regenerate *in vivo* [15–17]. Mature podocytes have elaborate basal membrane extensions (foot processes), which are linked together by specialized junctions (slit diaphragms), and interdigitate around glomerular capillaries to form a sieve-like filter for the blood [18–20]. Failure to properly form or maintain these structures results in defective urine production, which can be fatal [21–23]. hPSC-podocytes express several markers associated with podocytes, such as WT1, podocalyxin, synaptopodin, and nephrin, suggesting that these cells may be useful for disease modeling experiments and possibly cell therapy [4, 5, 24].

To establish the validity of this new system and advance the field, it is important to determine the developmental stage of hPSC-podocytes and their ability to phenocopy genetic disease. Microarray datasets of purified hPSC-podocytes show significant overlap with published mouse and human datasets, but the top genes do not cluster clearly with kidney tissues [24]. The rounded, tightly clustered appearance of hPSC-podocytes also differs markedly from that of cultured podocytes, which adopt a flat, enlarged morphology with irregular edges [15]. hPSC-podocytes can form extensions from their basal plasma

membranes, suggested to represent ‘primary’ or ‘secondary’ foot processes, but it is not clear whether they possess definitive, interdigitating, tertiary foot processes typical of mature podocytes *in vivo* [4, 13, 24]. Gene-edited hPSCs lacking podocalyxin (*PODXL*$^{-/-}$) exhibit defects in junctional organization and podocyte adhesion, providing the first evidence that hPSC-podocytes have potential to model disease [5]. However, ultrastructural analysis of these hPSC-podocytes has not been performed, and the mechanisms underlying these defects and their relevance to podocyte development *in vivo* are not yet clear.

To address these gaps, we perform here a detailed, quantitative comparison of hPSC-podocytes with developing podocytes *in vivo,* including *PODXL*$^{-/-}$ mutants and mouse models. Our work demonstrates that hPSC-podocytes resemble podocytes *in vivo* at the capillary loop stage (CLS) of glomerular development, and reveal a new role for podocalyxin-induced microvilli in this critical stage of differentiation.

MATERIALS AND METHODS

Kidney organoid differentiation and fixation

Cell lines included WA09 ESCs (WiCell; female), WTC11 iPSCs (Gladstone Institute; male), and *NPHS1-GFP* 201B7 iPSCs (Kumamoto University; female). Passages used were between 30 and 60. Kidney organoid differentiation was performed as described previously [5]. hPSCs were plated at a density of 45,000 cells/well in mTeSR1 (Stem Cell Technologies) + 10 μM Y27632 (LC Laboratories) on glass plates (LabTek) coated with 3 % GelTrex (Thermo Fisher Scientific) (day -3), which was changed to 1.5 % GelTrex in mTeSR1 (day -2), mTeSR1 (day -1), RPMI (Thermo Fisher Scientific) + 12 μM CHIR99021 (Tocris) (day 0), RPMI + B27 supplement (Thermo Fisher Scientific) (day 1.5), and fed every 2–3 days to promote kidney organoid differentiation. Organoids were fixed on day 18, unless otherwise noted. To fix, an equal volume of PBS (Thermo Fisher Scientific) + 8 % paraformaldehyde (Electron Microscopy Sciences) was added to the media for fifteen minutes, and the sample was subsequently washed three times with PBS. Kidneys (days 60–120) were obtained from the Laboratory of Developmental Biology (UW) with informed consent and approval of the institutional review board. To generate cryosections, halved kidneys were fixed in PBS + 4 % paraformaldehyde for one hour, incubated overnight in 30 % sucrose (Sigma) in water, mounted in Tissue-Tek (Sakura), and flash frozen with liquid nitrogen. For paraffin sections, tissues were fixed overnight with methacarn: 60 % absolute methanol, 30 % chloroform, 10 % glacial acetic acid (Sigma), and subsequently paraffin-embedded. Paraffin tissue sections were deparaffinized with three 2-minute washes in xylene, followed by 100 %, 85 %, and 70 % ethanol, and heated in citrate buffer pH 6.0 (Sigma) in a pressure cooker (Instant Pot IPDUO60) for three minutes prior to immunostaining.

Immunofluorescence

For immunofluorescence, fixed organoid cultures or tissue sections were blocked in 5% donkey serum (Millipore) + 0.3% Triton-X-100/PBS, incubated overnight in 3% bovine serum albumin (Sigma) + PBS with primary antibodies, washed, incubated with Alexa-Fluor secondary antibodies (Invitrogen), washed, and stained with DAPI or mounted in

Vectashield H-1000. Labels included fluorescein-labeled LTL (Vector Labs FL-1321, 1:500 dilution) and primary antibodies targeting ZO-1 (Invitrogen 339100, 1:100), hPODXL (R&D AF1658, 1:500), SYNPO (Santa Cruz sc-21537, 1:100), NPHS1 (R&D AF4269, 1:500), NPHS2 (Abcam ab50339, 1:300), PAX2 (Abnova H00005076-M01, 1:100), PAX8 (Proteintech 10336-1-AP, 1:300), and WT1 (Santa Cruz sc-192, 1:100). For PAX2, PAX8, and WT1, paraffin sections were used to determine localization patterns *in vivo.* Some cytoplasmic staining of these transcription factors was also observed, which was likely an artifact. Antibodies for PAX2 and PAX8 may show some cross-reactivity. Images are representative of stainings from three or more separate experiments.

Electron microscopy

Kidney organoid cultures were fixed in PBS + 4 % paraformaldehyde for five minutes, collected by scraping, pelleted at 300 *g*, and resuspended in EM fix: 0.15 M sodium cacodylate trihydrate (Sigma) dissolved in water (pH 7.3) containing 4% formaldehyde and 2% glutaraldehyde (Electron Microscopy Sciences). Kidney tissues (1 mm diameter) were placed directly into EM fix. Samples were post-fixed with osmium tetroxide solution (Sigma), dehydrated in serial ethanol dilutions (Sigma), and embedded in epoxy resin. Ultrathin sections (80 nm) were mounted on 200 mesh copper grids, stained with uranyl acetate and lead citrate (Electron Microscopy Sciences), and imaged with JEOL JEM-1010 and FEI Tecnai G2 Spirit TEMs. Images were representative of at least two kidneys containing numerous glomeruli per condition.

Image quantification and statistical analysis

Line scans of equivalent length were drawn basal to apical through representative cells and the raw fluorescence intensity values were averaged for each point along the line scan. For TEM images, microvillus density was measured for cells that had a clear apico-lateral surface by counting microvilli along this surface and dividing by its perimeter, without analyzing the basement membrane or foot processes. Cell separation was measured between two cell bodies that were directly adjacent to each other with nothing in-between by drawing a line between their two lateral membranes at a site of approximately median separation between the two cells' midlines. Foot processes were defined as continuous membrane events proximal to the glomerular basement membrane (GBM) on the side of the Bowman's space, that were separated by a slit diaphragm. The number of foot processes was counted and normalized to the length of the adjacent GBM. Statistical analysis was performed using a two-tailed *t* test for samples with unequal variance (heteroscedastic) between the wild-type and mutant cohorts.

Generation of podocalyxin mutants

Gene-edited *PODXL*$^{-/-}$ hPSCs and isogenic control lines were generated from WA09 hESCs [5]. Strains were backcrossed onto a C57Bl/6 background for at least 8 generations (F8). Germline Podxl-null mice (*Podxl*$^{-/-}$) and wild-type (WT) (+/+) control embryos were generated by intercrossing *Podxl*$^{+/-}$ mice [21]. The "floxed" *Podxl* mouse strain (*Podxl*$^{fl/fl}$) was generated as described [25]. For the *Podxl.Cdh5Cre* strain, *Podxl*$^{fl/+}$*Cre*$^{+/+}$ sires were crossed with *Podxl*$^{fl/fl}$*Cre*$^{+/+}$ dams to generate pups with *Podxl*$^{fl/fl}$*Cre*$^{+/+}$ ("Het") or *Podxl*$^{fl/+}$*Cre*$^{+/+}$ genotypes ("KO"). For the *Podxl.TekCre* strain, *Podxl*$^{fl/fl}$*Cre*$^{+/-}$ sires were

crossed with *Podxl*$^{+/-}$ *Cre*$^{-/-}$ dams to generate pups with the following genotypes: *Podxl*$^{fl/+}$*Cre*$^{+/-}$ (“Het”), *Podxl*$^{fl/-}$ *Cre*$^{+/-}$ (“KO”), *Podxl*$^{fl/+}$*Cre*$^{-/-}$ (“WT”) *and Podxl*$^{fl/-}$ *Cre*$^{-/-}$ (“WT”). Experiments using strains with conditional “floxed” alleles were performed using mice with Cre+ genotypes only (i.e., “Het” and “KO” genotypes) to control for potential Cre-expression effects.

Optical tweezers

Confluent hPSCs in a 35 mm dish were washed briefly with PBS and then cultured in Versene for 6 minutes and 30 seconds in the incubator, which was carefully aspirated from the edge of the well without detaching cells. 1 mL mTeSR1 + 10 μM Y27632 was added, triturated to detach cells, passed through a 40 μm filter, counted, and diluted to 2.3×10^4 cells/mL in 3 mL mTeSR1 + 6 μM Y27632 + 20 μL HEPES, and cells were transported on wet ice to the optical tweezers setup. Cells in solution were added into a 60 mm sterilized petri dish under an AXIO Imager D1m microscope (Zeiss). A 1064nm Nd:YVO_4 near-infrared laser and 50X objective lens (N.A.=0.55) were used to manipulate pairs of cells to the middle of the dish by optical tweezers, to avoid cell adhesion to the chamber surface. The pair of cells was placed as close as ~ 5 μm [26]. The laser was aimed in-between the two cells and activated at an intensity of 0.67 mW/μm^2 to attract them inwards. The distance between the two cells was measured when motion ceased. Experiments in which the cells became stuck to each other or to the chamber surface were excluded from the analysis.

RNA sequencing and analysis

RNA was prepared from isogenic sets of hPSCs using the RNEasy Mini Kit (Qiagen), checked for high integrity on an Agilent Bioanalyzer, and prepared using the TruSeq stranded mRNA library kit (Illumina). Samples were sequenced on an Illumina NextSeq500 75×75 paired end high output run and aligned to hg19 reference sequence. DESeq was used for differential gene expression analysis [27]. Two models were built. The null model assumed gene expression variation was purely due to experimental batches; the full model included mutant vs. control as an additional predictor. A gene was identified as significant when the full model fit was better (Benjamini-Hochberg FDR < 0.1). topGO R package was used for Gene Ontology enrichment analysis [28]. Ingenuity Pathway Analysis (Qiagen) was used to identify top upstream regulators. RNA-seq samples were deposited in the Gene Expression Omnibus (NCBI) under accession number GSE103547.

Electrostatic force calculation

Distance between cells ‘N’ and cell radius ‘r’ were calculated empirically by averaging TEM measurements. The isoelectric point (pI) of human podocalyxin was approximated by summing the logarithmic acid dissociation constant (pKa) values of the residues of the primary sequence. The number of sialic acids per podocalyxin molecule was estimated based on the literature [29]. Electrostatic force generated by podocalyxin was calculated assuming direct interference between perfectly opposite microvilli with ten podocalyxin molecules per microvillus, and did not include electrostatic contribution from neighboring microvilli which would account for a small increase in force (~ 10 % in two dimensions). As different microvillus arrangements and neighboring charges would increase electrostatic

interference, our force calculation is likely to be an underestimate. Application of Gauss' law yielded the same value as Coulomb's law.

RESULTS

hPSC-podocytes express markers of CLS podocytes

We utilized an adherent culture protocol to differentiate hPSCs into kidney organoids [5], in which proximal tubules and hPSC-podocytes could be distinguished using *Lotus tetragonolobus* lectin (LTL) and podocalyxin, respectively (Figure 1A and Supplemental Figure S1A–B). Tubule-like cells bordering and encapsulating podocyte clusters did not express podocalyxin, but also exhibited weaker LTL binding affinity compared to the proximal tubule (Figure 1A). Time course analyses confirmed that tubules and podocytes arose from aggregates of $SIX2^+$ nephron progenitor cells after 2–3 weeks in culture, concomitant with an upregulation of WT1, consistent with our previous characterization of this differentiation pathway (Supplemental Figure S1C–D). In lineage reporter hPSCs [24], green fluorescent protein (GFP) was expressed from the nephrin (NPHS1) locus in hPSC-podocytes (Figure 1B).

To determine the developmental stage of hPSC-podocytes, we directly compared gene expression and localization between kidney organoids *in vitro* and kidney organs. During organogenesis, podocytes first become detectable in primitive nephrons called S-shaped bodies (SSBs), and subsequently mature in CLS glomeruli [18]. We identified SSBs and CLS glomeruli in tissue sections from human kidneys and assessed these for expression and localization of nephrin and podocin (NPHS2), components of the slit diaphragm [22, 23]. Nephrin was expressed in podocytes of both SSBs and CLS glomeruli, whereas podocin was restricted to CLS glomeruli (Figure 1C). Both proteins strongly co-localized at the GBM, and were absent in neighboring tubular cells (Figure 1C–D). In kidney organoids, nephrin and podocin were enriched in linear, basement membrane-like tracks at the basal side of hPSC-podocytes (Figure 1C). Quantification of intensity peaks for nephrin and podocin revealed that they overlapped in hPSC-podocytes, similar to their patterns *in vivo* in CLS podocytes (Figure 1D).

Podocalyxin is a heavily sialylated member of the CD34 protein family that is highly expressed in podocytes *in vivo* and in hPSC-podocytes [5, 21, 29]. In primary tissue sections from SSBs and CLS glomeruli, podocalyxin localized exclusively to the apical surface of podocytes, contrasting with the basement membrane localization of nephrin and podocin (Figure 1E). Similarly, in kidney organoids, podocalyxin localized to the apical cell surface of hPSC-podocytes (Figure 1E). In both hPSC-podocytes and CLS podocytes, the intensity peaks of podocalyxin and podocin did not overlap and were found on opposite sides of the cell (Figure 1F).

The transcription factors paired box 2 (PAX2) and PAX8 are downregulated during podocyte specification, whereas WT1 is upregulated and linked to nephrin expression [30–33]. Previously, in RT-PCR analyses of whole kidney organoid cultures, PAX2 and WT1 were found to be co-expressed, raising the question of whether PAX genes were appropriately downregulated in hPSC-podocytes [5]. To distinguish between tubular and podocyte PAX

gene expression, we performed immunofluorescence analysis. In both SSBs and CLS glomeruli, PAX2 and PAX8 exhibited similar staining patterns, with bright nuclear immunofluorescence in tubules (Figure 1G–H). PAX2 and PAX8 immunofluorescence was absent in the nuclei of nephrin^{+} podocytes at both stages, although co-localization with nephrin was occasionally observed at the outer edges of podocyte clusters, where they bordered tubules (Figure 1G–H). Similarly, in kidney organoids, tubular cells expressed PAX2 and PAX8 in nuclei, while neighboring hPSC-podocytes downregulated these genes except where bordering tubules (Figure 1G–H). Thus, sustained expression of PAX genes in whole organoid cultures reflected upregulation by tubular cells, not hPSC-podocytes. Conversely, WT1 was specifically expressed in the nuclei of nephrin^{+} cells in both human kidneys and human kidney organoids (Figure 2A–B and Supplemental Figure S1D). Nephrin and WT1 were specific to the podocytes in organoids and were not expressed in neighboring tubules (Figure 2B). Collectively, these data indicated that marker expression and localization in hPSC-podocytes resembles CLS podocytes *in vivo*.

Junctions migrate basally in hPSC-podocytes

An unusual feature of podocyte maturation is the migration of tight junction components, such as ZO-1, from the apical to the basement membrane [18–20]. We first confirmed this localization pattern in human kidneys. In SSBs, immature podocytes could be identified based on their low, but detectable, co-expression of nephrin and WT1 (Figure 2A). ZO-1 localized to the sub-apical plasma membrane of these cells, similar to its expression in the tubule (Figure 2A). In CLS glomeruli, however, ZO-1 localization switched from the apical to the basement membrane (Figure 2A and Supplemental Figure S2A). Line scan quantification confirmed this relocation of the ZO-1 intensity peak from apical to basal, with an average migrational distance of approximately 10 μm (Figure 2A).

In kidney organoids, we identified a population of columnar, WT1-positive, polarized epithelial cells with low but detectable nephrin expression (nephrin^{lo} WT1^{+} ZO1^{+}) that formed a continuous epithelium with clusters of hPSC-podocytes expressing the same markers with higher nephrin levels (Figure 2B). Along this linear continuum, ZO-1 localization gradually migrated from the apical surface of nephrin^{lo} cells to the basal surface of nephrin^{hi} cells (Figure 2B and Supplemental Figure S2B). Basal localization of ZO-1 was strongly enriched within the nephrin^{hi} portion of the epithelium, corresponding to a rounded rather than columnar epithelial morphology (Figure 2B and Supplemental Figure S2B). Line scan analysis revealed the overall migrational distance of ZO-1 to be approximately 12 μm within this epithelium (Figure 2B). We further examined junctional organization during the time course of podocyte differentiation. Young hPSC-podocytes (day 11 of differentiation) formed epithelial layers one single cell in thickness, with a characteristic ellipsoid morphology. ZO-1 localized to lateral and sub-apical foci in these cells, whereas the slit diaphragm marker synaptopodin (SYNPO) was enriched at the basement membrane (Supplemental Figure S2C). At later time points (day 18 and onwards), podocytes formed paired layers whose basement membranes were connected by zipper-like tracks containing both synaptopodin and ZO-1 (Supplemental Figure S2C). These findings suggested that apical-to-basal migration of ZO-1 is recapitulated during the maturation of hPSC-podocytes

in vitro, resulting in their self-organization into conjoined layers at later stages of differentiation.

Ultrastructure of hPSC-podocytes in kidney organoids

We further analyzed these structures by transmission electron microscopy (TEM) to determine their cellular ultrastructure at day 18, a time point at which hPSC-podocytes adopted a mature appearance by immunofluorescence. In organoid cultures, tubular cells exhibited a columnar morphology and made direct contacts along their lateral plasma membranes to form a smooth-edged epithelium (Figure 3A). Tight junctions formed between these cells at their sub-apical surface, adjacent to the tubular lumen (Figure 3A). In contrast to the columnar morphology of the tubules, hPSC-podocytes formed clustered aggregates of rounded cells containing prominent nuclei with scant cytoplasm, and were readily detected by their distinct morphology (Figure 3A).

Within these aggregates, hPSC-podocytes were arranged intermittently along basement membrane-like tracks (Figure 3A). Neighboring hPSC-podocytes did not form close contacts between their lateral plasma membranes. Rather, numerous microvilli projected outwards from the lateral membranes, filling the spaces between cells (Figure 3A). A stalk-like cell body containing mitochondrial cristae and organelles connected each cell to the basement membrane, where junction-like structures were observed at points of cell-cell contact (Figure 3A). Basal to these junctions, hPSC-podocytes extended membranous processes, but robust interdigitating foot processes were not observed (Supplemental Figure S3A).

These findings were compared to TEM of human kidneys. As podocytes matured into CLS glomeruli, microvilli appeared between them in intercellular spaces (Figure 3B). CLS podocytes bore a striking resemblance to hPSC-podocytes, with apical nuclei, apical and lateral microvilli, scant cytoplasm, and a common basement membrane (Figure 3A–B). Similar cellular architectures were also observed in prenatal mouse kidneys, which contained immature glomeruli (Supplemental Figure S3B). In contrast to these, podocytes from adult mice exhibited distinctive, interdigitating foot processes and slit diaphragms (Supplemental Figure S3C).

Podocalyxin regulates microvillus formation and cell spacing in podocytes

To complement descriptive studies, we investigated whether hPSC-podocytes could provide new insights into the genetic mechanisms of CLS podocyte maturation. We therefore performed ultrastructural analysis on hPSC-podocytes derived from *PODXL*$^{-/-}$ hPSCs, which exhibit defects in junctional organization by confocal microscopy but have not previously been examined with TEM [5]. Surprisingly, ultrastructural analyses using TEM revealed that *PODXL*$^{-/-}$ hPSC-podocytes exhibited a near-total lack of microvilli, compared to non-mutant controls (Figure 4A). This reduction in microvilli was accompanied by a reduction in the lateral spaces between adjacent *PODXL*$^{-/-}$ hPSC-podocytes, and, correspondingly, an increase in the formation of lateral cell-cell junctions, which were rarely observed in control hPSC-podocytes of identical genetic background (Figure 4A). Quantification of these phenotypes revealed the changes in microvillus number and lateral

cell-to-cell distance to be approximately ten-fold and five-fold in magnitude, respectively (Figure 4B–C). Confocal imaging of hPSC-podocytes further revealed that apical microvilli in hPSC-podocytes contained podocalyxin (Figure 4D).

Our observation that podocalyxin was required for podocyte microvillus formation was a novel finding, which was not previously described in podocalyxin-deficient (*Podxl*$^{-/-}$) mice [21]. To validate hPSC-podocytes as a genetic model of CLS development, it was therefore important to determine whether this phenotype observed in human podocytes *in vitro* was also true of CLS podocytes *in vivo.* To investigate the role of podocalyxin *in vivo,* we generated new *Podxl*$^{-/-}$ mice and analyzed microvillus formation in the glomeruli of these animals. As *Podxl*$^{-/-}$ mice die of anuria shortly after birth [21], prenatal mice (E18.5) were examined (Figure 5A). TEM analyses of glomeruli in *Podxl*$^{-/-}$ mice showed a drastic decrease in the ability of podocytes to form microvilli, compared to littermate controls (Figure 5B–C). Spacing between adjacent *Podxl*$^{-/-}$ podocytes was likewise greatly decreased (Figure 5B,D). *Podxl*$^{-/-}$ mouse podocytes *in vivo* therefore phenocopied *PODXL*$^{-/-}$ hPSC-podocytes *in vitro,* demonstrating that hPSC podocytes could reveal genetic mechanisms of CLS maturation.

In addition to podocytes, podocalyxin is also expressed in endothelial cells (ECs), where it can affect vascular permeability [25, 34]. To determine the effect of podocalyxin on glomerular ECs, we generated mice lacking podocalyxin specifically in the vasculature. Using two different lineage reporters, these mice were healthy and viable with no obvious phenotype unless vascular leak was induced [25]. We detected no difference in the morphology of glomerular ECs or podocytes by TEM (Figure 6A and Supplemental Figure S4A–B). Quantitative analysis revealed no differences in podocyte microvillus or foot process formation (Figure 6B and Supplemental Figure S4C–D). In human kidney organoids, hPSC-podocytes were not identified solely on the basis of podocalyxin expression, but rather as tightly clustered, rounded cells that co-expressed synaptopodin, nephrin, podocin, and podocalyxin, at much higher levels than any other cells in the organoid or surrounding cells in the culture. hPSC-derived ECs also arose within kidney organoid cultures, as previously reported, but could be readily distinguished from hPSC-podocytes based on the expression of specific markers such as CD31, and by their chain-like networks, which extended beyond the organoid into the surrounding stroma [5]. Podocalyxin expression in hPSC-ECs was dramatically lower than in neighboring hPSC-podocytes, consistent with our previous report (Figure 6C) [5]. Collectively, these data suggested that the kidney defects we observed in podocalyxin mutants were due to podocalyxin loss in podocytes, rather than in ECs.

The finding that podocalyxin induced microvillus formation, and localized to these microvilli, suggested that it might promote cell separation by establishing an anti-adhesive surface. To test this, we performed experiments using optical tweezers [26]. As hPSC-podocytes are terminally differentiated cells that cannot be readily purified or expanded, these experiments were performed on undifferentiated hPSCs, which strongly express podocalyxin. Control or *PODXL*$^{-/-}$ hPSCs were first dissociated to disrupt cell junctions, and were subsequently trapped in pairs using a laser to determine their minimum separation distance (Figure 7A). Under controlled laser power, *PODXL*$^{-/-}$ hPSCs consistently

exhibited cell separation distances ~ 50 % lower than control hPSCs (Figure 7B). As this anti-adhesive effect occurred within a time frame of seconds and in the absence of pre-formed junctions, it suggested that steric or electrostatic alterations in membrane surface composition were responsible.

We further performed global gene analysis (RNA-Seq) to identify differentially expressed genes and pathways in *PODXL*$^{-/-}$ and control hPSCs. The top gene ontology terms enriched in *PODXL*$^{-/-}$ hPSCs were related to positive regulation of cell-cell adhesion (Figure 7C). Podocalyxin itself was among the top differentially expressed genes (Figure 7D). In addition to podocalyxin itself, this analysis suggested the possible involvement of additional factors, including ZFP28 and OLIG2, and upstream regulators, such as HNF1A and OTX2, not previously associated with podocalyxin (Figure 7D–E). Interestingly, among the top upstream regulators was CLIC4, an intracellular chloride channel that is required for microvillus assembly in retinal pigmented epithelial cells, where it associates with ezrin and the actin cytoskeleton (Figure 7E) [35]. A close homolog, CLIC5, is strongly expressed in podocytes and is associated with microvilli and podocalyxin [36]. Collectively, these unbiased experiments suggested critical roles for podocalyxin in regulating cell adhesion and microvillus formation, likely through both direct and indirect pathways.

DISCUSSION

Podocytes have been challenging to study in culture systems, due to their tendency to dedifferentiate and limited proliferative capacity [15–17]. hPSC-podocytes arise naturally in kidney organoids in large clusters are therefore an attractive candidate for *in vitro* studies [3–5, 24]. Although hPSC-podocytes can be clearly discerned within organoids, their appearance and gene expression patterns are different from those of cultured primary and immortalized podocytes [15, 24]. A detailed comparison of hPSC-podocytes to developing podocytes *in vivo* has not previously been performed, which has made it difficult to determine the developmental stage of these cells and their utility for disease modeling and kidney regeneration. Our findings, which directly compare kidney organoids to mouse and human podocytes in tissue sections, reveal that hPSC-podocytes attain a differentiation state and specialized cytoskeletal architecture in cell culture that resembles CLS podocytes *in vivo.* Gene-edited hPSC-podocytes further reveal ultrastructural defects, which can be recapitulated in transgenic mouse embryos at this stage of development. Thus, perceived differences between organoid hPSC-podocytes and primary podocytes reflect differences in developmental stage or isolation conditions, rather than cell type. Interestingly, our analysis also suggests the presence of transitional cells in-between the podocyte and proximal tubular compartments, which express a distinct combination of markers ($PAX2^{+}PAX8^{+}LTL^{lo}PODXL^{-}$). The precise identity of these cells is an interesting topic for further investigation.

How podocytes establish their specialized architecture during CLS podocyte maturation is not clear from studies *in vivo*. Our TEM analysis reveals for the first time that endogenous podocalyxin is required for efficient microvillus formation in podocytes, both in humans and in mice. Our experiments using optical tweezers further indicate that podocalyxin directly affects the adhesiveness of adjacent cell surfaces in a rapid, context-independent manner.

Collectively, these findings suggest a model in which podocalyxin directly induces apical-to-basal junctional migration (Figure 7F). Podocalyxin localizes to the apical and lateral cell membranes of podocytes, where it induces the localized formation of microvilli via the actin-binding protein ezrin [37, 38]. The strong negative charge on podocalyxin [29] promotes electrostatic repulsion between microvilli on adjacent cells (Figure 7G). Application of Coulomb's law, together with empirical data from Figure 4 and the literature, reveals that for two cells separated by 0.73 μm, the electrostatic force generated by podocalyxin is ~ 1 nanonewton, and reaches ~ 13 nanonewtons at a distance of 0.2 μm which is typical of *PODXL*$^{-/-}$ hPSC-podocytes (Figure 7H–I). These forces are sufficiently strong to repel and separate adjacent cellular membranes from their adhesive interactions [39, 40]. The separation of lateral membranes induces the regional dissolution of cell-cell junctions, which are limited to remaining points of cell-cell contact at the basal membrane. In podocalyxin mutants, repulsion between adjacent membranes is greatly reduced, preventing them from separating and leading to retention of junctions along their interface and blocked filtration of urine into tubules (Figure 7F). This model provides novel insight into how junctions are restricted to the basal membranes of podocytes, a critical first step in foot process formation. Anti-podocalyxin antibodies developed for use in cancer and hPSC provide a possible tool for drug delivery or purification of podocytes for therapeutic purposes [41, 42].

A key question is whether kidney organoids and hPSC-podocytes *in vitro* can accurately phenocopy disease states *in vivo*. Our study suggests that loss-of-function mutations in human *PODXL* would likely cause embryonic or perinatal lethality, similar to mice [21]. This might explain why the incidence of podocalyxin mutations in living patients with kidney disease is relatively low [43]. In this regard, our collaborators (laboratories of Drs. Murim Choi and Hae Il Chong at the Seoul National University College of Medicine, Seoul, Republic of South Korea) recently identified a human neonatal patient with two loss-of-function mutations in *PODXL* – each allele inherited from heterozygous parents. The patient, who unfortunately died at infancy (~ 4 months), presented with severe nephrotic syndnrome and omphalocele – characteristics similar to the major defects detected in *Podxl*-deficient mice (Kang and Lee *et al.*, manuscript submitted). Thus, both genetic data from patients and our culture assays suggest a highly conserved function for *PODXL* in mammalian development.

Our findings demonstrate that hPSC-podocytes *in vitro* complete the process of junctional migration but do not go on to form *bona fide* foot processes with tertiary interdigitations. Additional factors are therefore required for podocyte maturation. In this regard, it is striking that hPSC-podocytes form epithelial bilayers that are fused together at their basement membranes. To establish a GBM, one of these podocyte layers must be replaced with a layer of ECs, which may be a key missing factor. Although kidney organoids contain ECs, they are relatively low in abundance, and may lack specialized characteristics required for proper pairing with hPSC-podocytes, such as specific laminin isoform expression [44]. An important future direction is therefore to carefully characterize this hPSC-EC compartment and identify ways to further enhance and specialize it to better mimic developing capillary loops *in vivo*.

CONCLUSION

In conclusion, comparative analysis of hPSC-podocytes *in vitro* and developing CLS podocytes *in vivo* indicates that these are highly similar cell types. Gene-edited hPSC-podocytes reveal mechanisms of glomerular development at this stage, which are further validated in knockout mice. The accessibility of hPSC-podocytes to experimental manipulation and imaging establishes an attractive model for deciphering the regulatory cues that guide podocyte specialization, with future potential for glomerular regeneration.

Supplementary Material

Refer to Web version on PubMed Central for supplementary material.

Acknowledgments

We thank Ed Parker (UW) for TEM, Ryan Vander werff (UBC) for transcriptomics, Ryuichi Nishinakamura (Kumamoto University) for NPHS1-GFP cells, Jonathan Himmelfarb (UW) and Jennifer Harder (University of Michigan) for discussions, and support from NIH K01DK102826 (BSF), R01DK097598, UH2DK107343 (SJS), K25HL135432 (HF), P01GM081619 (YW), R24HD000836 (Laboratory of Developmental Biology), National Kidney Foundation Young Investigator Grant (BSF), American Society of Nephrology Carl W. Gottschalk Research Scholar Award (BSF), Natural Sciences and Engineering Research Council of Canada RGPIN155397-13 (AWV), and National Science Foundation IDBR DBI-1353718 (LYL).

References

1. Barak H, Huh SH, Chen S, et al. FGF9 and FGF20 maintain the stemness of nephron progenitors in mice and man. Dev Cell. 2012; 22:1191–1207. [PubMed: 22698282]
2. Brown AC, Muthukrishnan SD, Oxburgh L. A synthetic niche for nephron progenitor cells. Dev Cell. 2015; 34:229–241. [PubMed: 26190145]
3. Taguchi A, Kaku Y, Ohmori T, et al. Redefining the in vivo origin of metanephric nephron progenitors enables generation of complex kidney structures from pluripotent stem cells. Cell Stem Cell. 2014; 14:53–67. [PubMed: 24332837]
4. Takasato M, Er PX, Chiu HS, et al. Kidney organoids from human iPS cells contain multiple lineages and model human nephrogenesis. Nature. 2015; 526:564–568. [PubMed: 26444236]
5. Freedman BS, Brooks CR, Lam AQ, et al. Modelling kidney disease with CRISPR-mutant kidney organoids derived from human pluripotent epiblast spheroids. Nat Commun. 2015; 6:8715. [PubMed: 26493500]
6. Dekel B, Burakova T, Arditti FD, et al. Human and porcine early kidney precursors as a new source for transplantation. Nat Med. 2003; 9:53–60. [PubMed: 12496960]
7. Xinaris C, Benedetti V, Rizzo P, et al. In vivo maturation of functional renal organoids formed from embryonic cell suspensions. J Am Soc Nephrol. 2012; 23:1857–1868. [PubMed: 23085631]
8. Unbekandt M, Davies JA. Dissociation of embryonic kidneys followed by reaggregation allows the formation of renal tissues. Kidney Int. 2010; 77:407–416. [PubMed: 20016472]
9. Rogers SA, Lowell JA, Hammerman NA, et al. Transplantation of developing metanephroi into adult rats. Kidney Int. 1998; 54:27–37. [PubMed: 9648060]
10. Thomson JA, Itskovitz-Eldor J, Shapiro SS, et al. Embryonic stem cell lines derived from human blastocysts. Science. 1998; 282:1145–1147. [PubMed: 9804556]
11. Takahashi K, Tanabe K, Ohnuki M, et al. Induction of pluripotent stem cells from adult human fibroblasts by defined factors. Cell. 2007; 131:861–872. [PubMed: 18035408]
12. Lam AQ, Freedman BS, Morizane R, et al. Rapid and efficient differentiation of human pluripotent stem cells into intermediate mesoderm that forms tubules expressing kidney proximal tubular markers. J Am Soc Nephrol. 2014; 25:1211–1225. [PubMed: 24357672]

13. Morizane R, Lam AQ, Freedman BS, et al. Nephron organoids derived from human pluripotent stem cells model kidney development and injury. Nat Biotechnol. 2015; 33:1193–1200. [PubMed: 26458176]
14. Mae S, Shono A, Shiota F, et al. Monitoring and robust induction of nephrogenic intermediate mesoderm from human pluripotent stem cells. Nat Commun. 2013; 4:1367. [PubMed: 23340407]
15. Saleem MA, O'Hare MJ, Reiser J, et al. A conditionally immortalized human podocyte cell line demonstrating nephrin and podocin expression. Journal of the American Society of Nephrology : JASN. 2002; 13:630–638. [PubMed: 11856766]
16. Kim YG, Alpers CE, Brugarolas J, et al. The cyclin kinase inhibitor p21CIP1/WAF1 limits glomerular epithelial cell proliferation in experimental glomerulonephritis. Kidney Int. 1999; 55:2349–2361. [PubMed: 10354282]
17. Ronconi E, Sagrinati C, Angelotti ML, et al. Regeneration of glomerular podocytes by human renal progenitors. J Am Soc Nephrol. 2009; 20:322–332. [PubMed: 19092120]
18. Reeves W, Caulfield JP, Farquhar MG. Differentiation of epithelial foot processes and filtration slits: sequential appearance of occluding junctions, epithelial polyanion, and slit membranes in developing glomeruli. Laboratory investigation; a journal of technical methods and pathology. 1978; 39:90–100. [PubMed: 682603]
19. Hartleben B, Schweizer H, Lubben P, et al. Neph-Nephrin proteins bind the Par3-Par6-atypical protein kinase C (aPKC) complex to regulate podocyte cell polarity. J Biol Chem. 2008; 283:23033–23038. [PubMed: 18562307]
20. Reiser J, Kriz W, Kretzler M, et al. The glomerular slit diaphragm is a modified adherens junction. J Am Soc Nephrol. 2000; 11:1–8. [PubMed: 10616834]
21. Doyonnas R, Kershaw DB, Duhme C, et al. Anuria, omphalocele, and perinatal lethality in mice lacking the CD34-related protein podocalyxin. J Exp Med. 2001; 194:13–27. [PubMed: 11435469]
22. Kestila M, Lenkkeri U, Mannikko M, et al. Positionally cloned gene for a novel glomerular protein--nephrin--is mutated in congenital nephrotic syndrome. Molecular cell. 1998; 1:575–582. [PubMed: 9660941]
23. Boute N, Gribouval O, Roselli S, et al. NPHS2, encoding the glomerular protein podocin, is mutated in autosomal recessive steroid-resistant nephrotic syndrome. Nature genetics. 2000; 24:349–354. [PubMed: 10742096]
24. Sharmin S, Taguchi A, Kaku Y, et al. Human Induced Pluripotent Stem Cell-Derived Podocytes Mature into Vascularized Glomeruli upon Experimental Transplantation. Journal of the American Society of Nephrology : JASN. 2016; 27:1778–1791. [PubMed: 26586691]
25. Debruin EJ, Hughes MR, Sina C, et al. Podocalyxin regulates murine lung vascular permeability by altering endothelial cell adhesion. PLoS One. 2014; 9:e108881. [PubMed: 25303643]
26. Jing P, Wu J, Liu GW, et al. Photonic Crystal Optical Tweezers with High Efficiency for Live Biological Samples and Viability Characterization. Sci Rep. 2016; 6:19924. [PubMed: 26814808]
27. Anders S, Huber W. Differential expression analysis for sequence count data. Genome Biol. 2010; 11:R106. [PubMed: 20979621]
28. Alexa A, Rahnenfuhrer J, Lengauer T. Improved scoring of functional groups from gene expression data by decorrelating GO graph structure. Bioinformatics. 2006; 22:1600–1607. [PubMed: 16606683]
29. Kerjaschki D, Vernillo AT, Farquhar MG. Reduced sialylation of podocalyxin--the major sialoprotein of the rat kidney glomerulus--in aminonucleoside nephrosis. Am J Pathol. 1985; 118:343–349. [PubMed: 3976840]
30. Ryan G, Steele-Perkins V, Morris JF, et al. Repression of Pax-2 by WT1 during normal kidney development. Development. 1995; 121:867–875. [PubMed: 7720589]
31. Bouchard M, Souabni A, Mandler M, et al. Nephric lineage specification by Pax2 and Pax8. Genes Dev. 2002; 16:2958–2970. [PubMed: 12435636]
32. Kann M, Ettou S, Jung YL, et al. Genome-Wide Analysis of Wilms' Tumor 1-Controlled Gene Expression in Podocytes Reveals Key Regulatory Mechanisms. J Am Soc Nephrol. 2015; 26:2097–2104. [PubMed: 25636411]
33. Guo G, Morrison DJ, Licht JD, et al. WT1 activates a glomerular-specific enhancer identified from the human nephrin gene. J Am Soc Nephrol. 2004; 15:2851–2856. [PubMed: 15504938]

34. Horrillo A, Porras G, Ayuso MS, et al. Loss of endothelial barrier integrity in mice with conditional ablation of podocalyxin (Podxl) in endothelial cells. Eur J Cell Biol. 2016; 95:265–276. [PubMed: 27289182]

35. Chuang JZ, Chou SY, Sung CH. Chloride intracellular channel 4 is critical for the epithelial morphogenesis of RPE cells and retinal attachment. Mol Biol Cell. 2010; 21:3017–3028. [PubMed: 20610659]

36. Wegner B, Al-Momany A, Kulak SC, et al. CLIC5A, a component of the ezrin-podocalyxin complex in glomeruli, is a determinant of podocyte integrity. Am J Physiol Renal Physiol. 2010; 298:F1492–1503. [PubMed: 20335315]

37. Nielsen JS, Graves ML, Chelliah S, et al. The CD34-related molecule podocalyxin is a potent inducer of microvillus formation. PLoS One. 2007; 2:e237. [PubMed: 17311105]

38. Takeda T, Go WY, Orlando RA, et al. Expression of podocalyxin inhibits cell-cell adhesion and modifies junctional properties in Madin-Darby canine kidney cells. Mol Biol Cell. 2000; 11:3219–3232. [PubMed: 10982412]

39. Krieg M, Arboleda-Estudillo Y, Puech PH, et al. Tensile forces govern germ-layer organization in zebrafish. Nat Cell Biol. 2008; 10:429–436. [PubMed: 18364700]

40. Thie M, Rospel R, Dettmann W, et al. Interactions between trophoblast and uterine epithelium: monitoring of adhesive forces. Hum Reprod. 1998; 13:3211–3219. [PubMed: 9853883]

41. Snyder KA, Hughes MR, Hedberg B, et al. Podocalyxin enhances breast tumor growth and metastasis and is a target for monoclonal antibody therapy. Breast Cancer Res. 2015; 17:46. [PubMed: 25887862]

42. Choo AB, Tan HL, Ang SN, et al. Selection against undifferentiated human embryonic stem cells by a cytotoxic antibody recognizing podocalyxin-like protein-1. Stem Cells. 2008; 26:1454–1463. [PubMed: 18356574]

43. Barua M, Shieh E, Schlondorff J, et al. Exome sequencing and in vitro studies identified podocalyxin as a candidate gene for focal and segmental glomerulosclerosis. Kidney international. 2014; 85:124–133. [PubMed: 24048372]

44. St John PL, Abrahamson DR. Glomerular endothelial cells and podocytes jointly synthesize laminin-1 and -11 chains. Kidney Int. 2001; 60:1037–1046. [PubMed: 11532098]

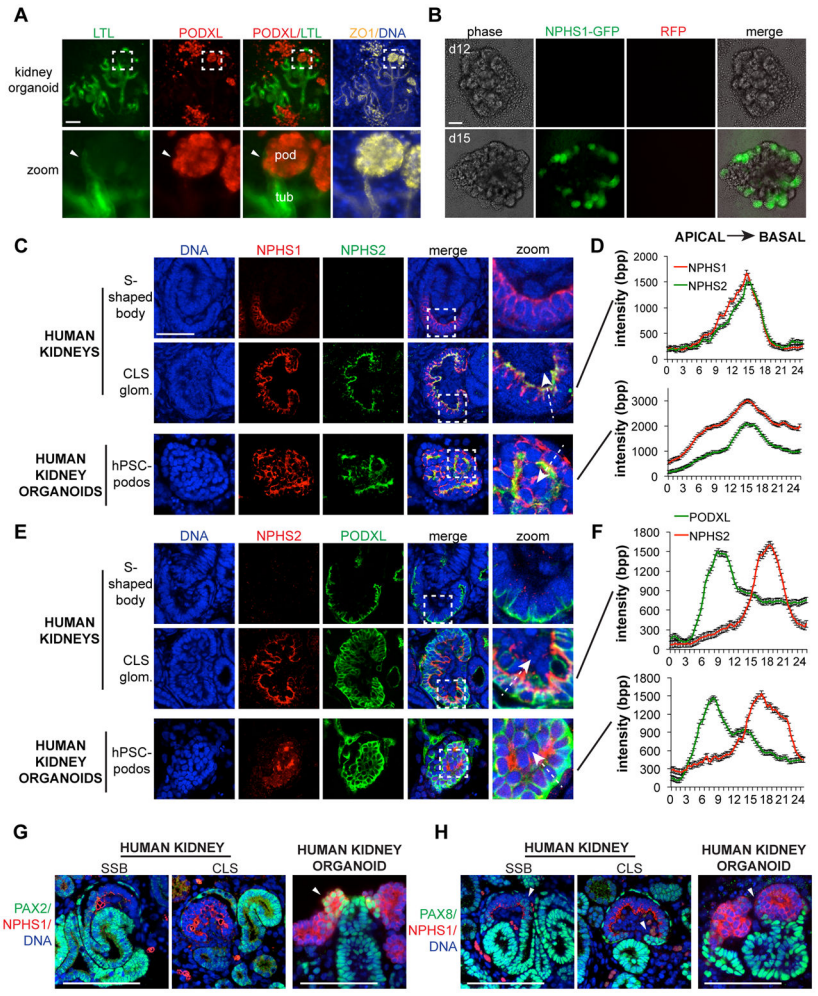

Figure 1. Marker localization in hPSC-podocytes and CLS podocytes

(A) Representative wide-field fluorescence image of kidney organoids showing tubule (LTL) and podocyte (PODXL) populations co-localized with the tight junction protein ZO-1. Zoom shows dashed white boxed region where a tubule (tub) forms a junction with a cluster of podocytes (pod). Arrowhead indicates tubule-like cells bordering the podocyte cluster. (B) NPHS1-GFP organoids on days 12 and 15 of differentiation. Red channel is included as a negative control for autofluorescence. (C) Representative confocal optical sections and (D) averaged raw fluorescence intensities in line scans drawn through podocytes, showing co-localization of podocin (NPHS2) with nephrin (NPHS1) or (E–F) with podocalyxin (PODXL) in human glomeruli and kidney organoids. Zoom of boxed regions are shown at right for the merged images. White dashed arrows demonstrate how line scans were drawn. Line scans are 24 μm through individual cells (n = 10). bpp, bits per pixel (raw intensities). (G) Representative confocal images of kidney tissues (left) or human kidney organoids (right) showing co-localization of nephrin with antibodies raised against PAX2 and (H) PAX8. Arrowheads indicate PAX2 or PAX8 co-localization with nephrin at the edge of the podocyte cluster. Scale bars, 100 μm.

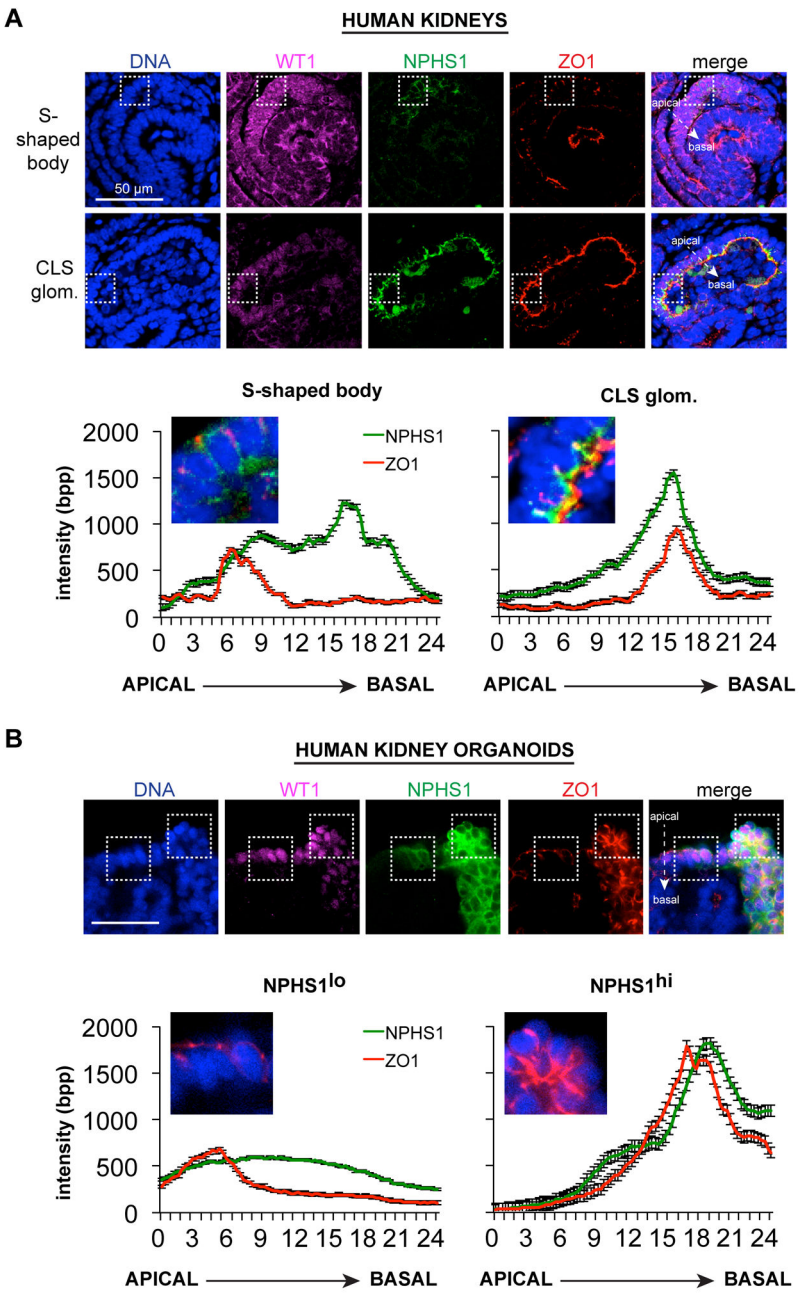

Figure 2. Junctions migrate basally during maturation of hPSC-podocytes and CLS podocytes

(A) Representative confocal optical sections (top) and averaged raw fluorescence intensity line scans (bottom) showing ZO-1 and NPHS1 localization in developing human kidneys and (B) human kidney organoids. Zoom of boxed regions without WT1 (human kidneys), or without WT1 and nephrin (human kidney organoids), are shown below images. Apical and basal sides of the epithelium are labeled in merged images. White dashed arrows demonstrate how line scans were drawn. Line scans are 24 µm through individual cells (n = 10). Y axes are the same throughout. Scale bars, 20 µm.

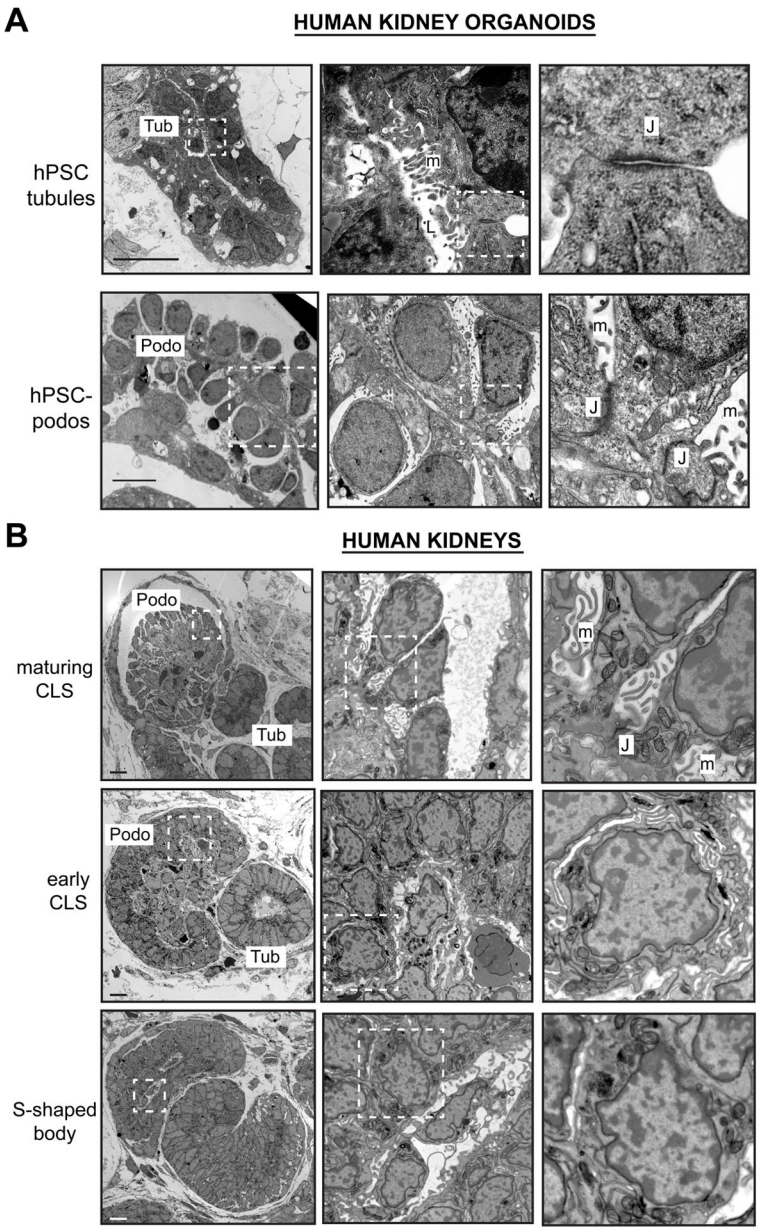

Figure 3. The ultrastructure of hPSC-podocytes resembles CLS podocytes *in vivo*

(A) Representative TEM images of tubules (Tub) and podocytes (Podo) in human kidney organoids. J, junctions; m, microvilli; L, lumen. Arrows indicate tubule-like cells bordering the podocyte aggregate. (B) Developing glomeruli at different stages in human kidneys. Note similarity between maturing CLS podocytes and hPSC-podocytes at highest magnification. Scale bars, 10 μm.

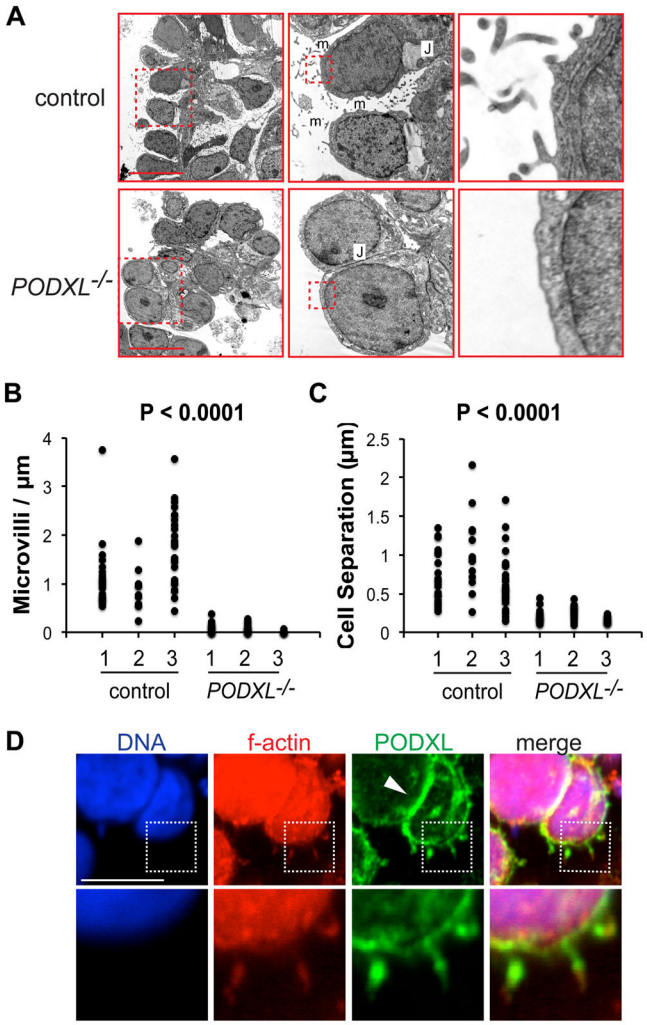

Figure 4. Podocalyxin regulates microvillus formation and cell spacing in hPSC-podocytes

(A) Representative TEM images of control and *PODXL*$^{-/-}$ hPSC-podocytes. Progressive zooms are shown for boxed regions in TEM images. m, microvilli; J, junctions. (B) Counts of microvillus number in *PODXL*$^{-/-}$ hPSC-podocytes, compared to non-mutant controls. Each point represents a single podocyte (n = 3 experiments). (C) Quantification of separation distance between cell lateral membranes in these hPSC-podocytes, with associated p-values. (D) Confocal section showing podocalyxin co-localization with filamentous actin at high magnification. Arrowhead highlights podocalyxin concentration between adjacent hPSC-podocytes. Boxed area is shown in zoom and highlights microvilli. Scale bars, 10 µm.

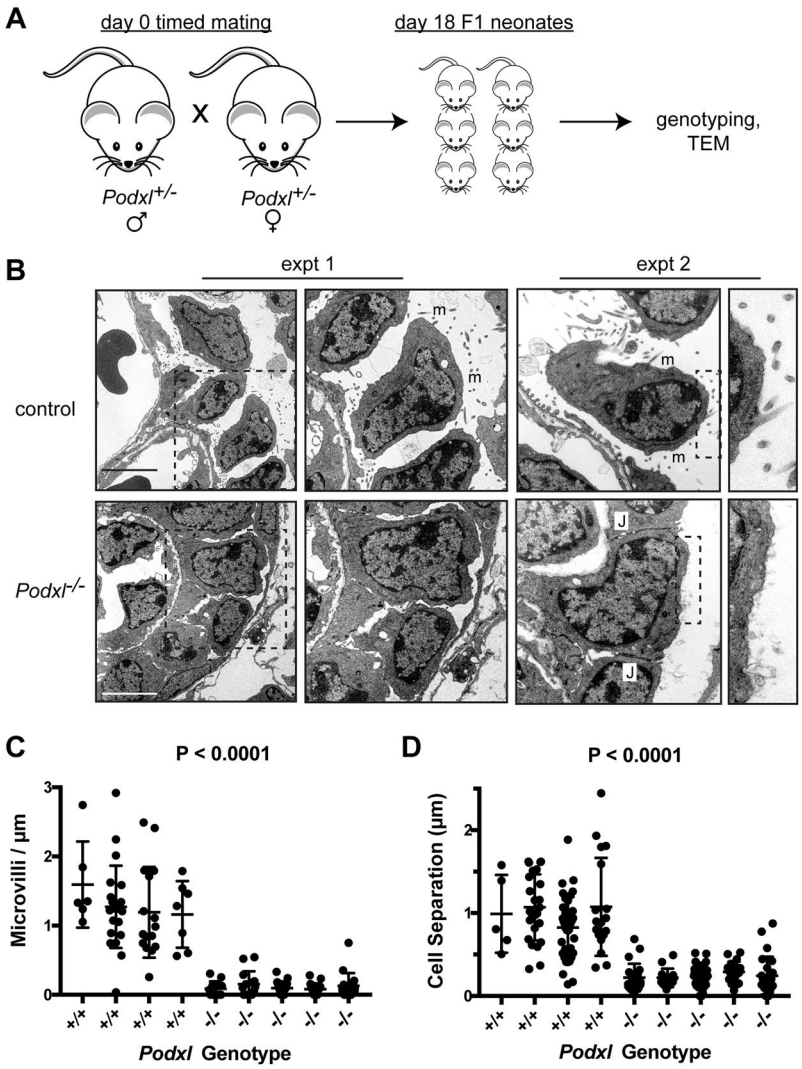

Figure 5. Podocalyxin regulates microvillus formation and cell spacing in mouse podocytes

(A) Schematic of knockout mouse generation and analysis. (B) TEM images of podocytes from *Podxl*$^{-/-}$ prenatal mice (E18.5), or age-matched littermate controls. Images from two representative experiments are shown. Zoom is shown to the right for dashed boxed regions. m, microvilli; J, junctions. (C) Quantification of microvillus number and (D) cell separation in *Podxl*$^{-/-}$ podocytes and littermate controls, with associated p-values. Each point represents a single podocyte (n = 4 control and 5 *Podxl*$^{-/-}$ mice). Scale bars, 5 µm.

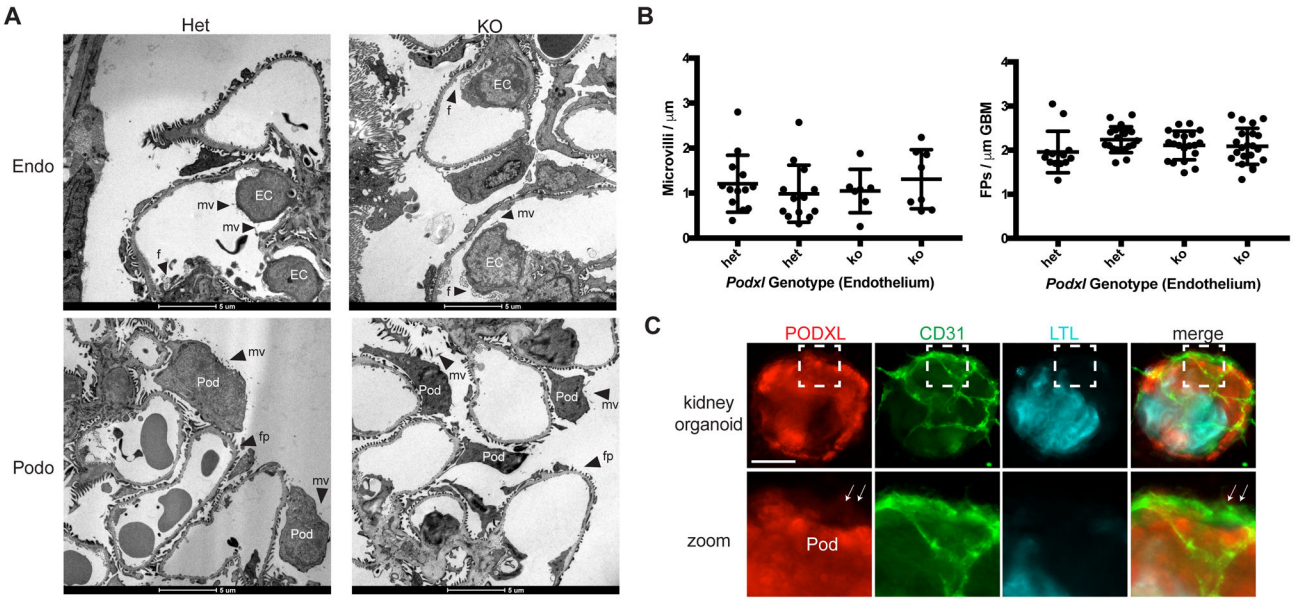

Figure 6. Loss of podocalyxin from endothelial cells does not significantly affect the morphology of glomerular endothelial cells or podocytes

(A) TEM micrographs of glomerular endothelial cells (endo) and podocytes (podo) in Cdh5-driven podocalyxin knockout mice, compared to controls. Fenestrae (f); microvillus (mv); foot process (fp); podocyte (Pod); endothelial cell (EC). (B) Quantification of microvillus formation (microvilli per unit length of apico-lateral membrane) iand foot process frequency (continuous membrane events proximal to the glomerular basement membrane separated by a slit diaphragm per length of unit basement membrane) in podocytes from Cdh5-Cre mice. (C) Representative wide-field immunofluorescence images of podocalyxin expression in kidney organoids containing endothelial cells (CD31) and proximal tubules (LTL). Zoom shows close-up of white dashed boxed region. Arrows indicated faint podocalyxin staining in endothelial cells, relative to the underlying layer of podocytes (Pod). Scale bars, 5 µm (A) or 100 µm (C).

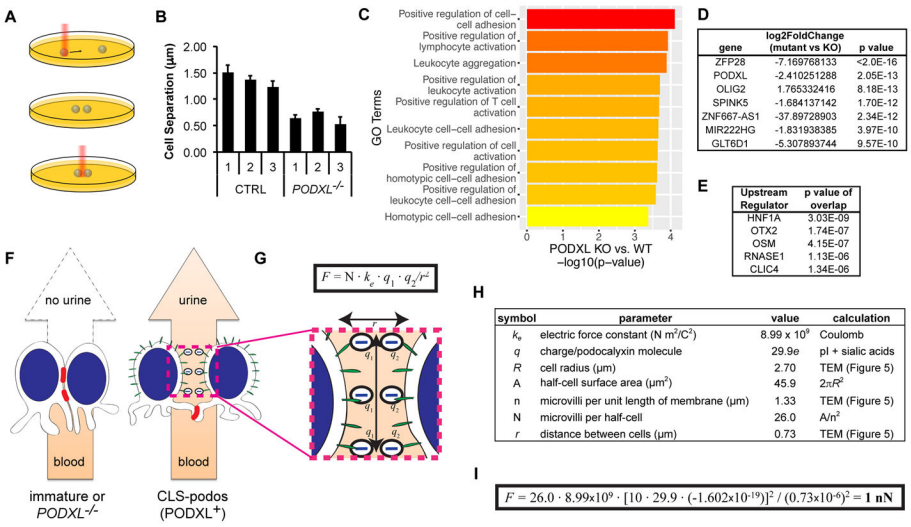

Figure 7. Podocalyxin increases cell-cell spacing

(A) Schematic of optical tweezers experiment. Steps are shown top to bottom. Cells are depicted as green spheres. (B) Quantification of gap widths measured with optical tweezers in control or *PODXL*$^{-/-}$ cells. Three distinct subclones are shown (average ± s.e.m., n ≥ 7 cells per subclone, p = 4.39 × 10^{-17}). (C) Top gene ontology terms, (D) differentially expressed genes, and (E) upstream regulators in PODXL$^{-/-}$ hPSCs, relative to isogenic controls. Data were obtained from three separate experiments (different days), each including 2–3 cell lines of each genotype. (F) Schematic of podocalyxin function. In the absence of podocalyxin, podocytes remain closely apposed and form lateral junctions through which urine cannot be filtered (left). During CLS maturation (right), podocalyxin-coated microvilli (green) form on the apical and lateral surfaces of podocytes. Sialic acid residues (negative charges) on podocalyxin act as an anti-adhesive, separating cell membranes and promoting basal migration of junctional complexes (red) to basal slits, through which urine is filtered. (G) Zoom-in of podocyte cell surfaces in close contact, showing the application of Coulomb's law. (H) Table of parameters for the estimation of surface area and microvillus charge for each membrane, with (I) accompanying charge calculation for two membranes containing ten podocalyxin molecules per microvillus.